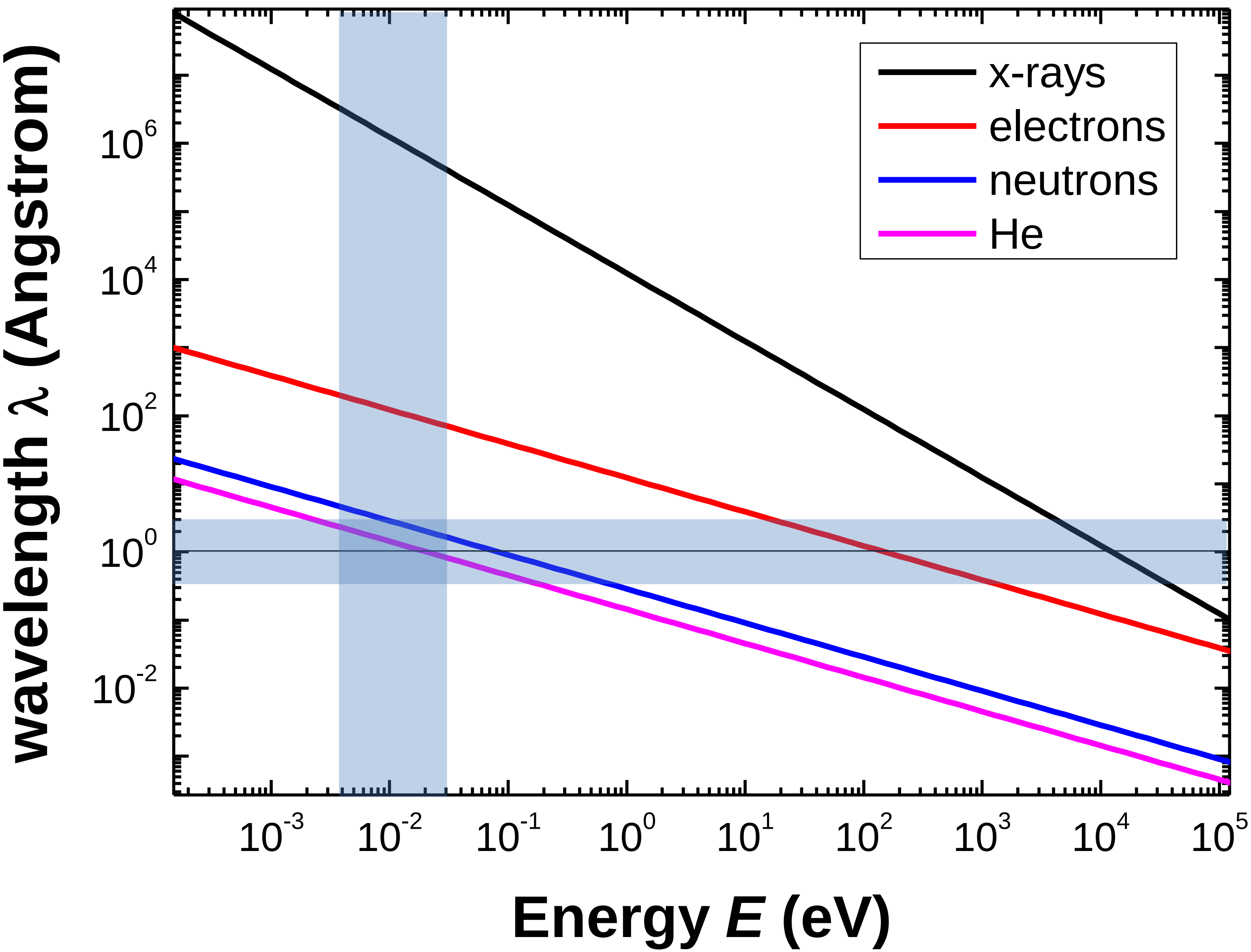

x-rays
electrons
neutrons
He
wavelength λ (Angstrom)
Energy E (eV)
10^6
10^4
10^2
10^0
10^-2
10^-3
10^-2
10^-1
10^0
10^1
10^2
10^3
10^4
10^5

Electron energy loss spectroscopy

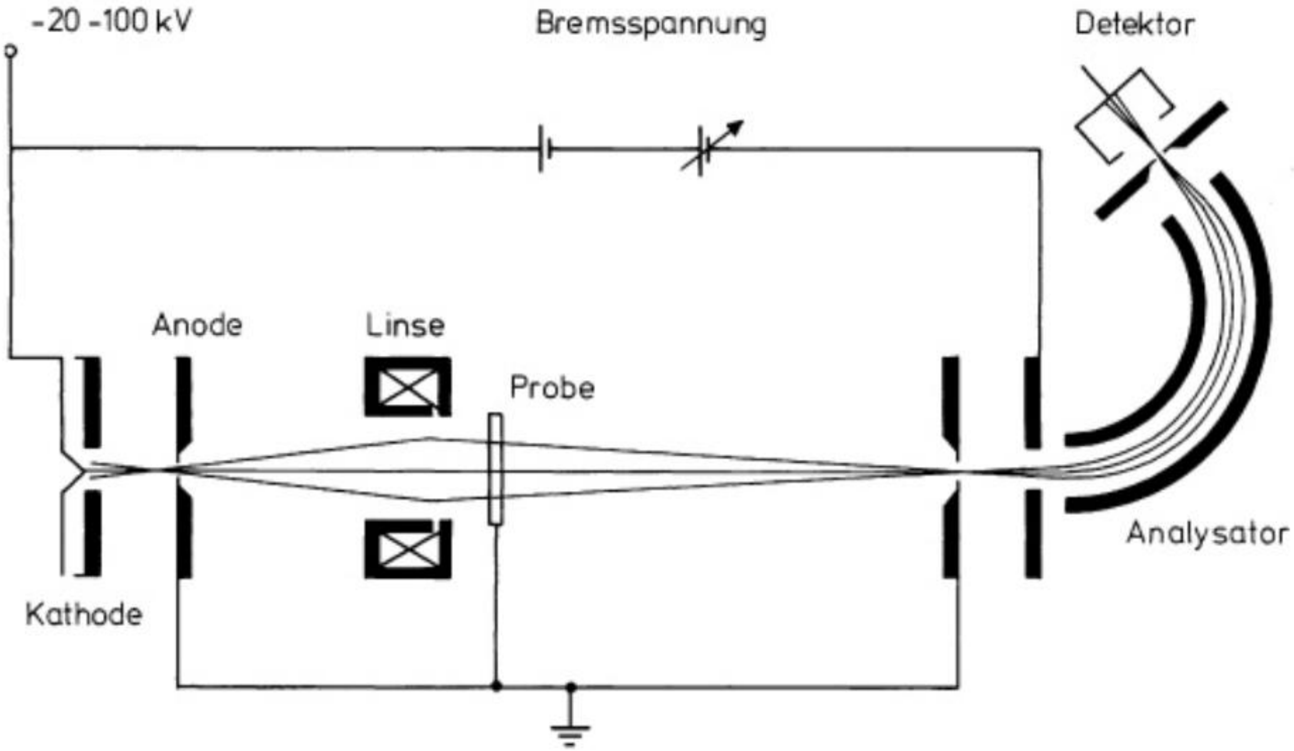

Abb. XI.2. Elektronenspektrometer für die Transmissionsspektroskopie. (Nach Raether [XI.4])

EELS - example

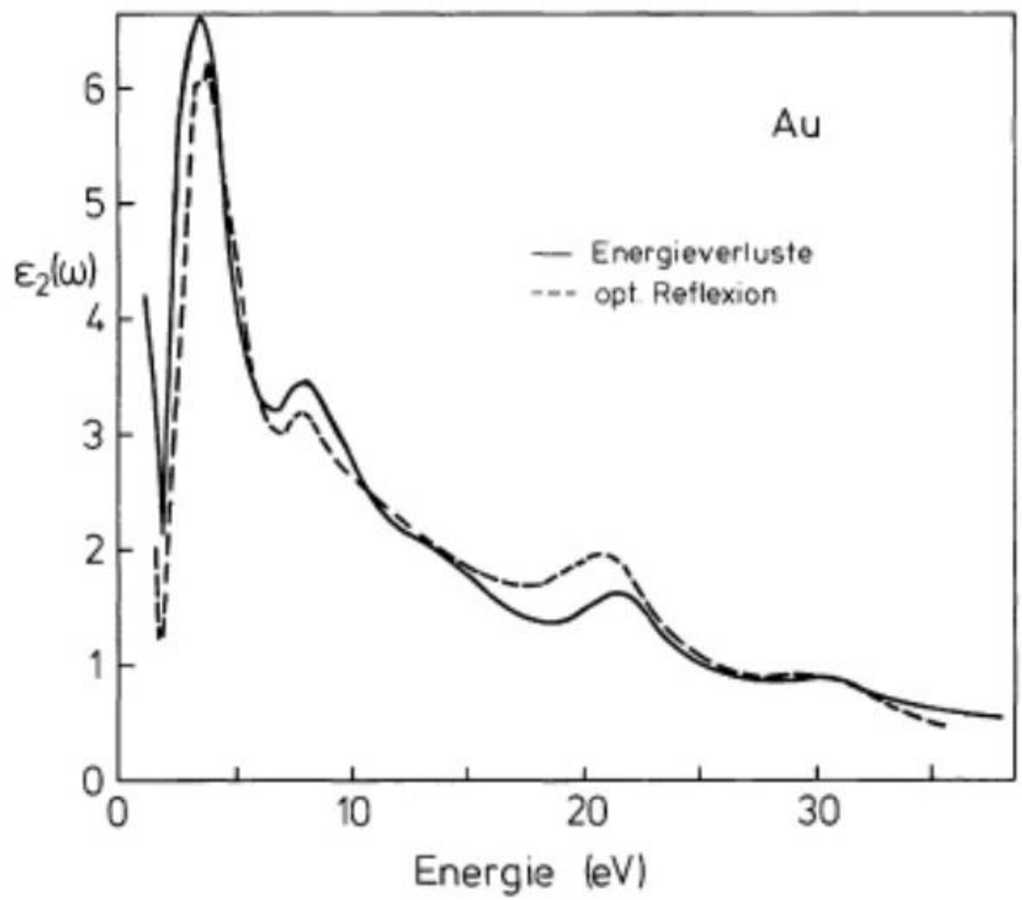

Abb. XI.3. Vergleich von $\varepsilon_2(\omega)$ für Gold aus Elektronenspektroskopie (*ausgezogene Linie*) und aus Messungen des optischen Reflexionsvermögens. (Nach Daniels et al. [XI.5])

EELS on Si(111) 7x7

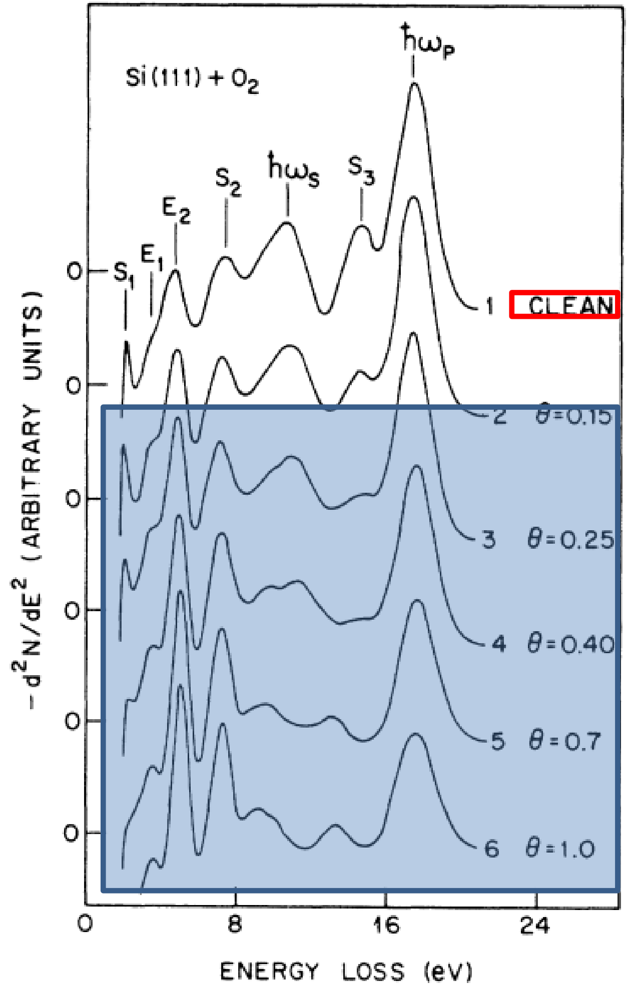

FIG. 2. Negative second derivative of the loss spectrum of a clean silicon (111)7×7 surface (curve 1) and spectra of increasing coverage with oxygen. Primary energy is 100 eV.

hw_p: bulk plasmon
hw_s: surface plasmon
E_1,E_2: bulk interband transitions
S_2,S_2,S_3: transitions from occupied surface states

HREELS

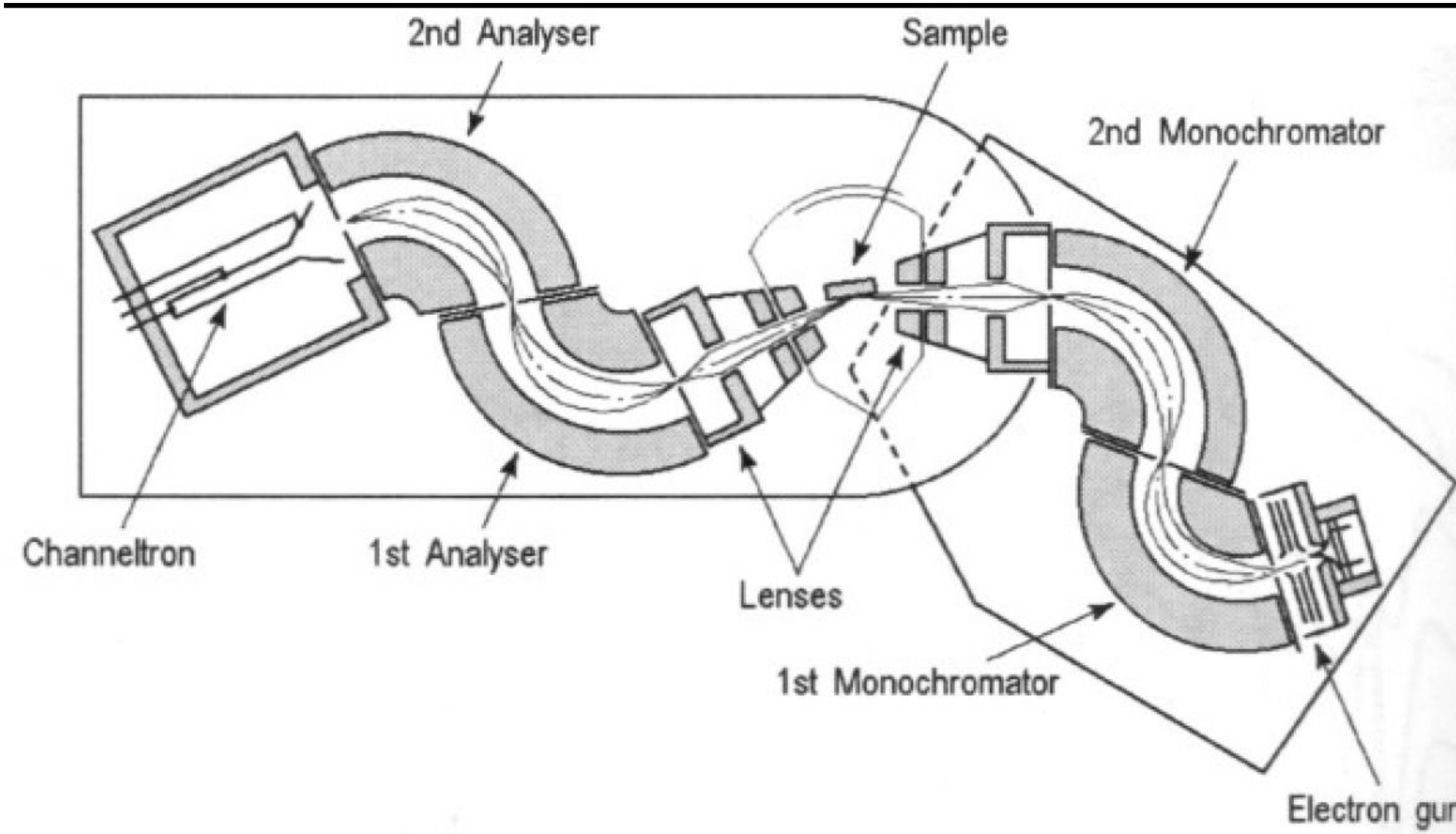

Fig. 5.15. A typical experimental set-up used for high-resolution electron energy loss spectroscopy. It comprises a cathode emission system, a monochromator, two lens systems, an analyzer, and an electron detector. Both analyzer and monochromator utilize 127°-angle cylindrical sector deflectors as the energy dispersive elements (after Ibach [5.11])

HREELS example: graphene

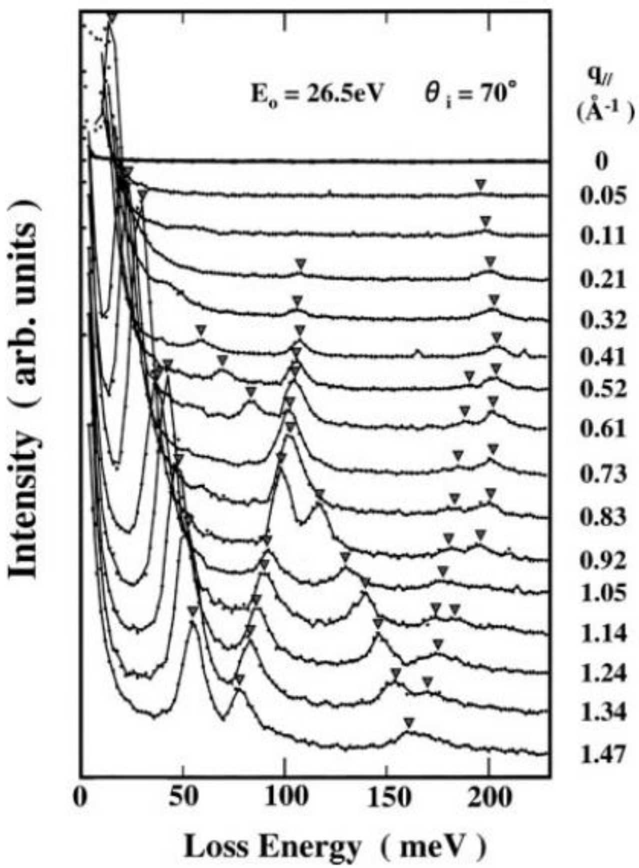

Figure 3. The HREEL spectra of graphene sheets on $BC_3/NbB_2(0001)$ measured along the $\Gamma - M$ direction in the surface Brillouin zone.

G-mode

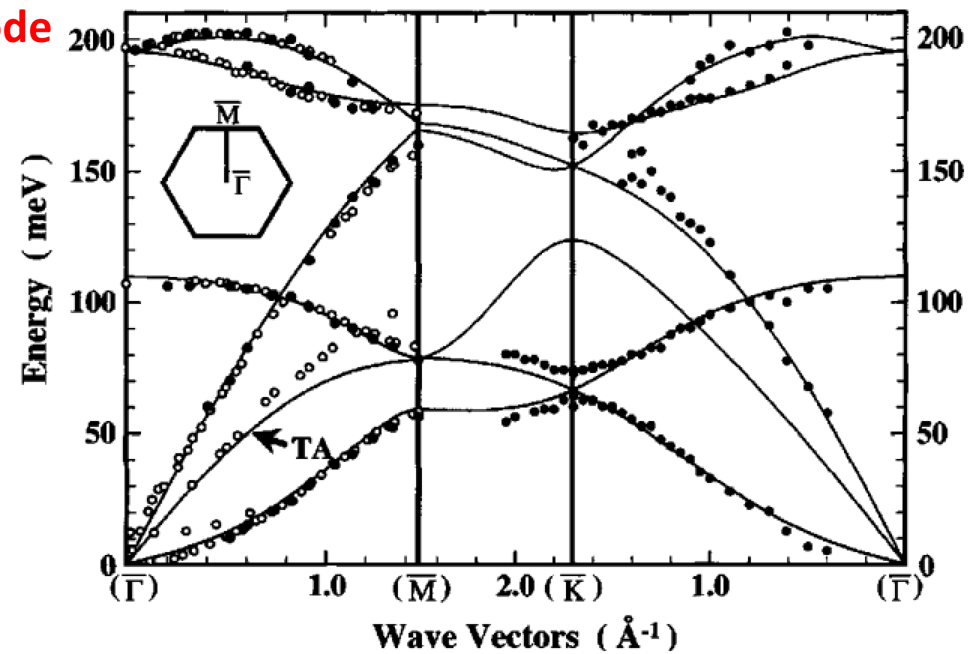

Figure 4. Phonon energy dispersion curves of the graphene sheets determined experimentally (solid circles) and theoretically (solid curves). Phonons in the bulk graphite surfaces are also shown for comparison (open circles).

Surface plasmon (polariton)

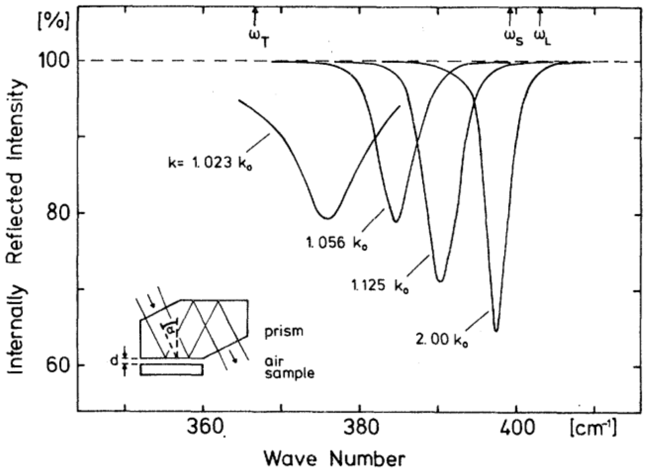

FIG. 1. Spectra of attenuated total reflection (parallel polarization) at room temperature. Different value of k according to Eq. (3). Spacings: $d = 40$, 25, 12, and 2.5μ m, ordered to increasing values of k. Inset shows experimental arrangement.

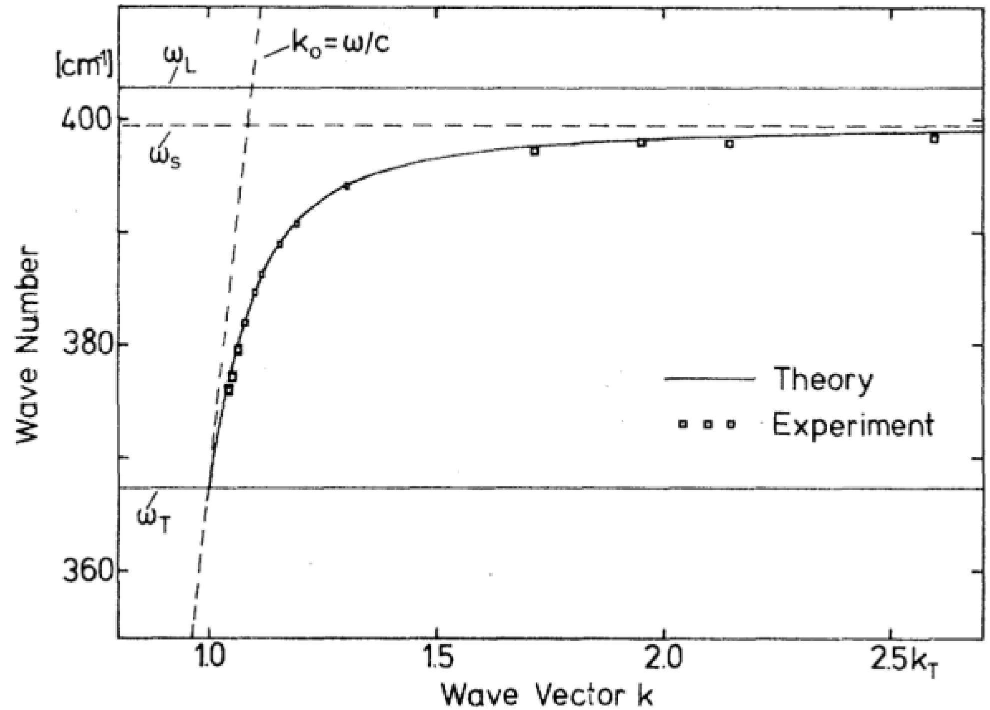

FIG. 2. Dispersion of surface polaritons in GaP. Experimental accuracy is given by size of rectangles. Theoretical curve is calculated from Eq. (1).

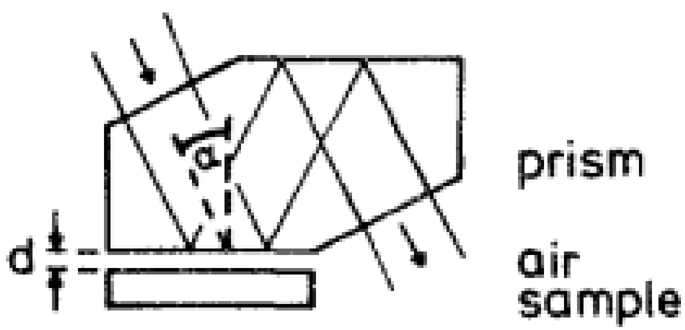

Types of magnetic order

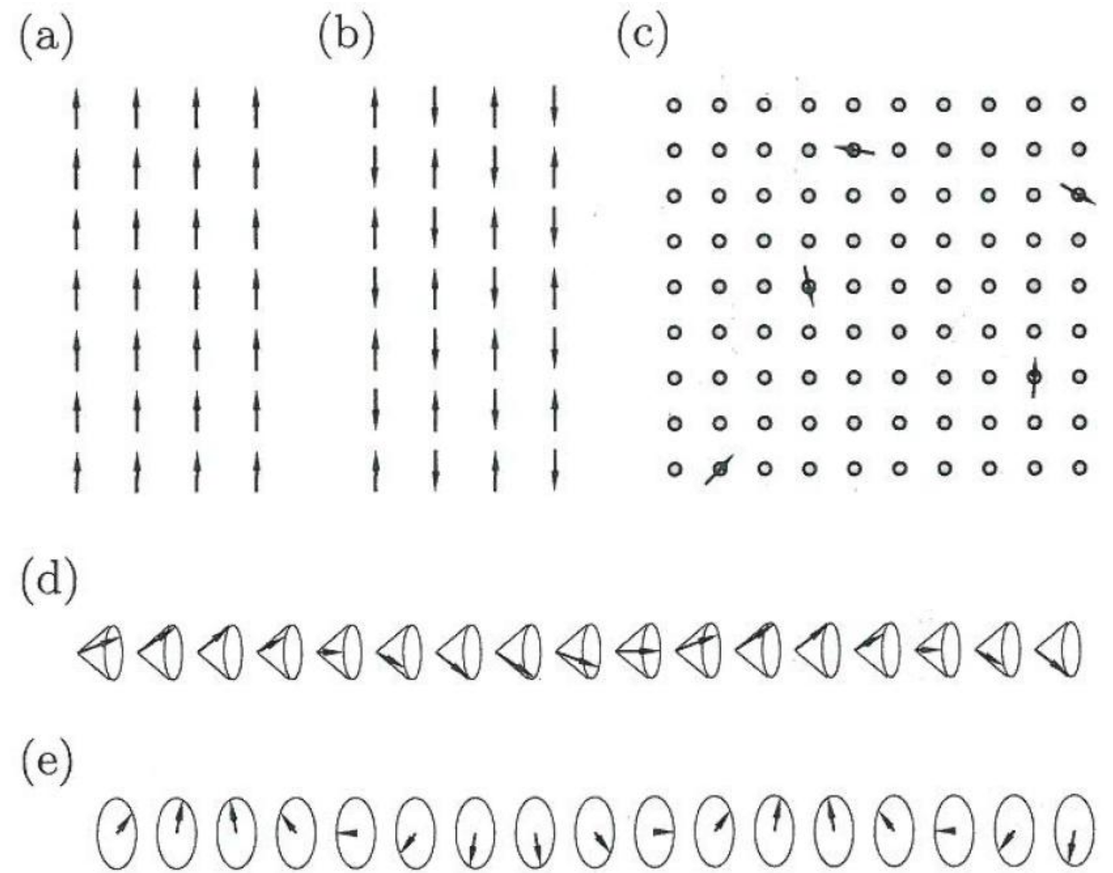

Fig. 5.1 Various spin arrangements in ordered systems: (a) ferromagnets, (b) antiferromagnets, (c) spin glasses and (d) spiral and (e) helical structures.

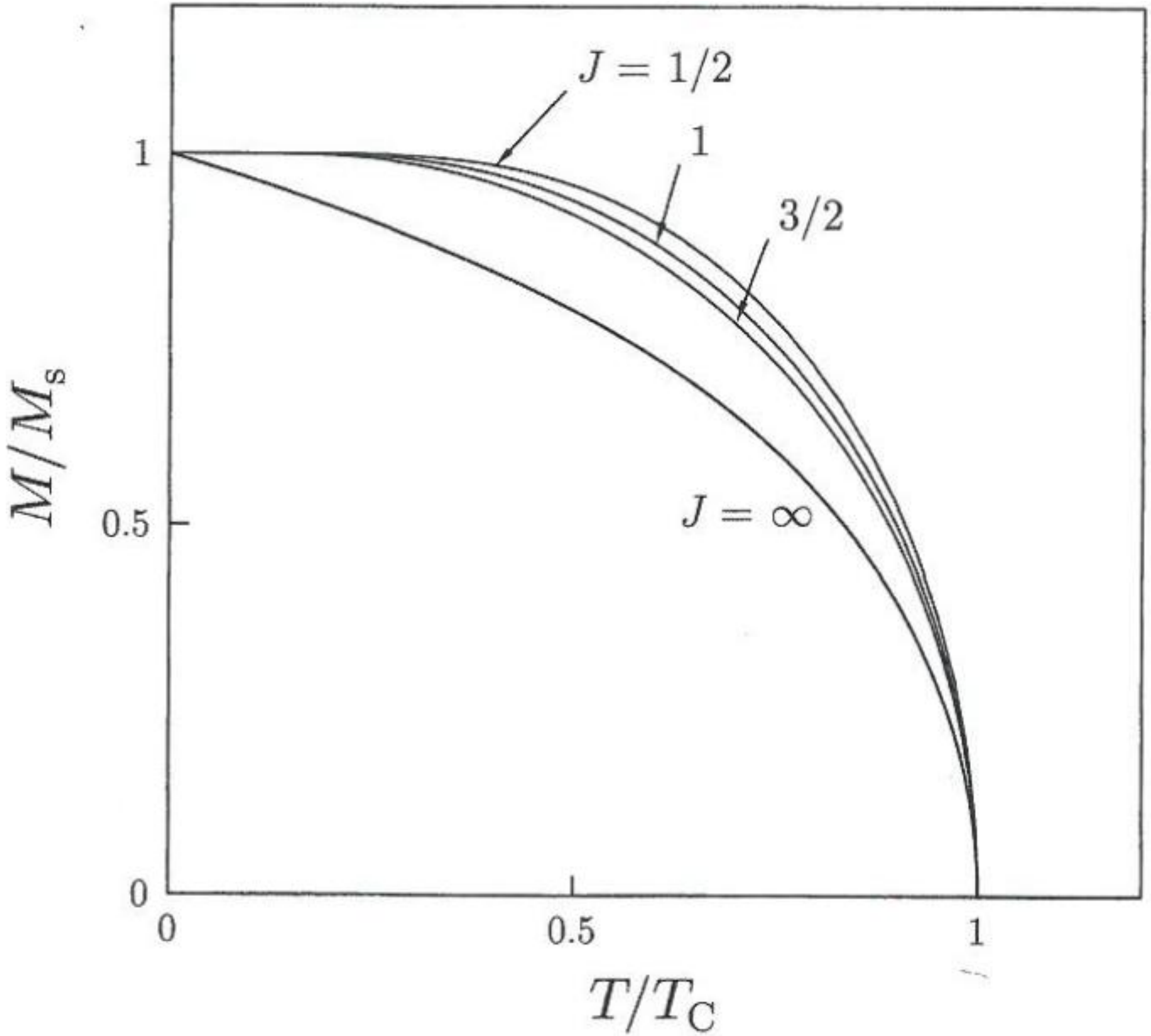

Fig. 5.3 The mean-field magnetization as a function of temperature, deduced for different values of J.

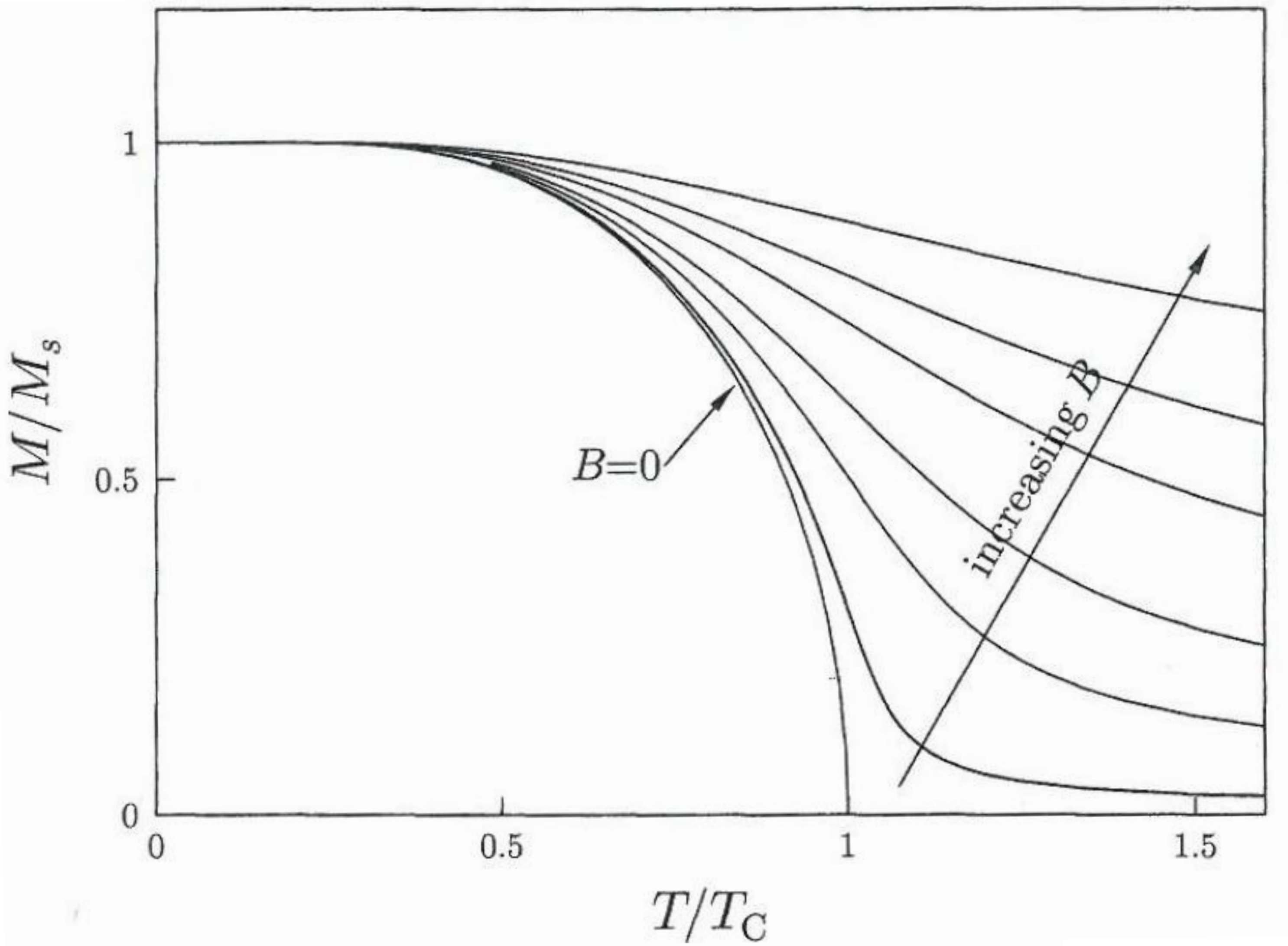

Fig. 5.5 The mean-field magnetization as a function of temperature for $J = \frac{1}{2}$, calculated for different values of the applied field B. The phase transition is only present when $B = 0$.

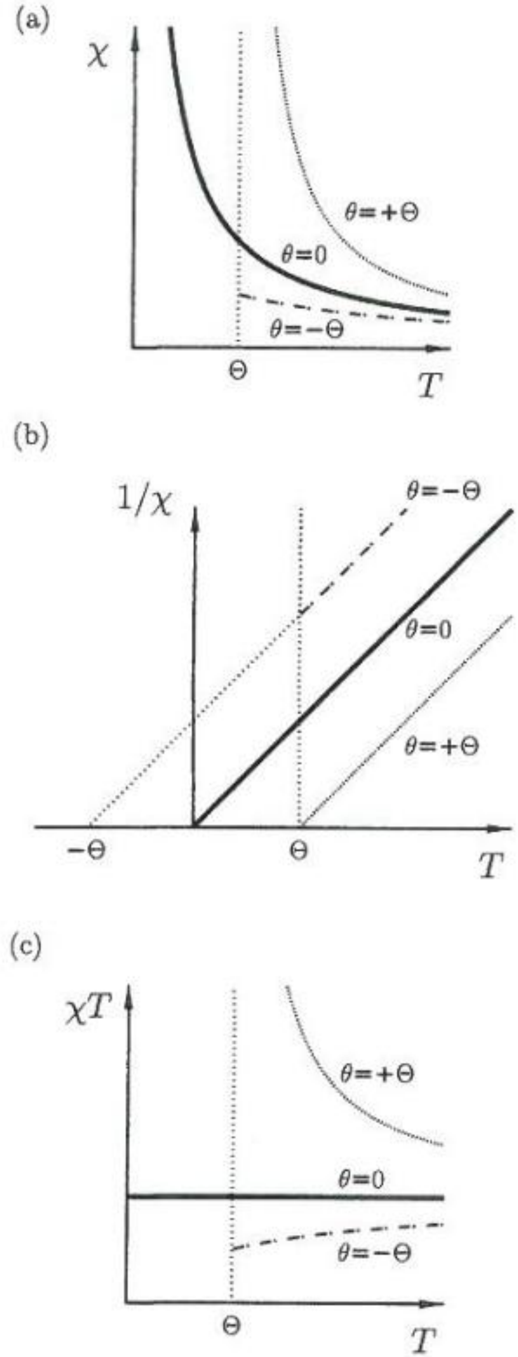

Fig. 5.7 The Curie Weiss law states that χ $1/(T-\theta)$ for $T > \theta$. This is shown in (a) f three cases: $\theta = 0$ (paramagnet), $\theta = \Theta >$ (ferromagnet) and $\theta = -\Theta < 0$ (antiferr magnet). Straight-line graphs are obtained l plotting $1/\chi$ against T as shown in (b) wi the intercept on the temperature axis yieldi θ. A graph of χT against T can be consta ($\theta = 0$), increasing for decreasing T ($\theta >$ or decreasing for decreasing T ($\theta < 0$), shown in (c).

Susceptibility of an antiferromagnet

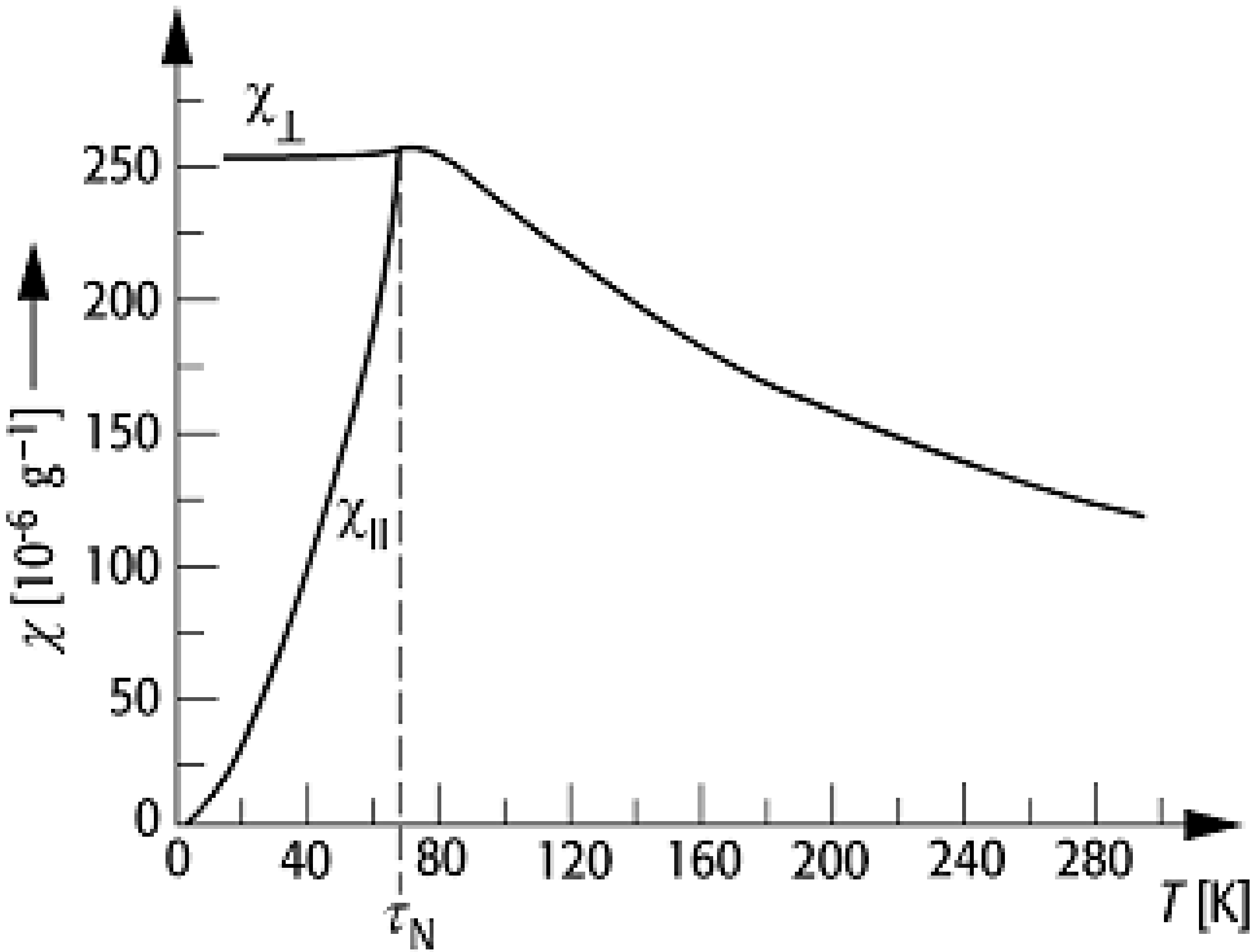

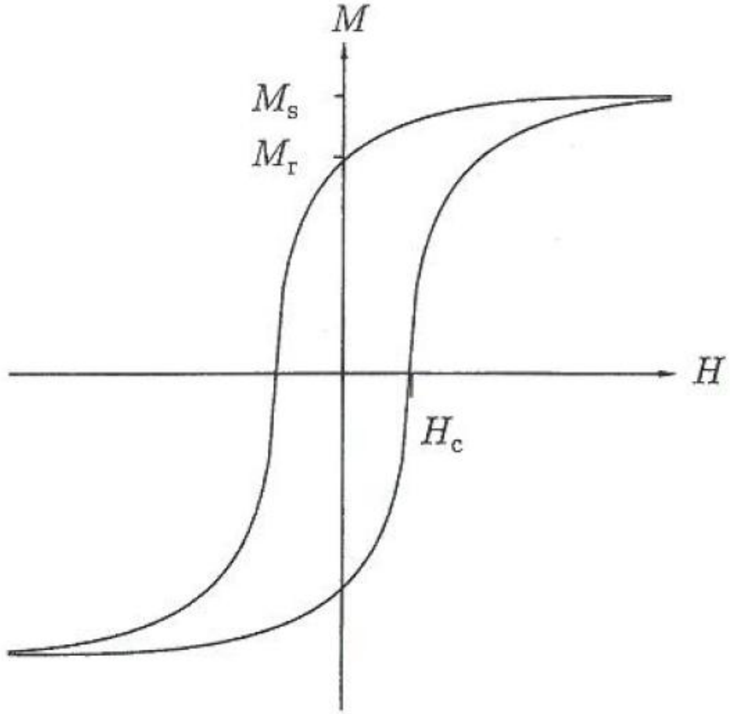

Fig. 6.24 A hysteresis loop showing the saturation magnetization M_S, the remanent magnetization M_r and the coercive field H_C.

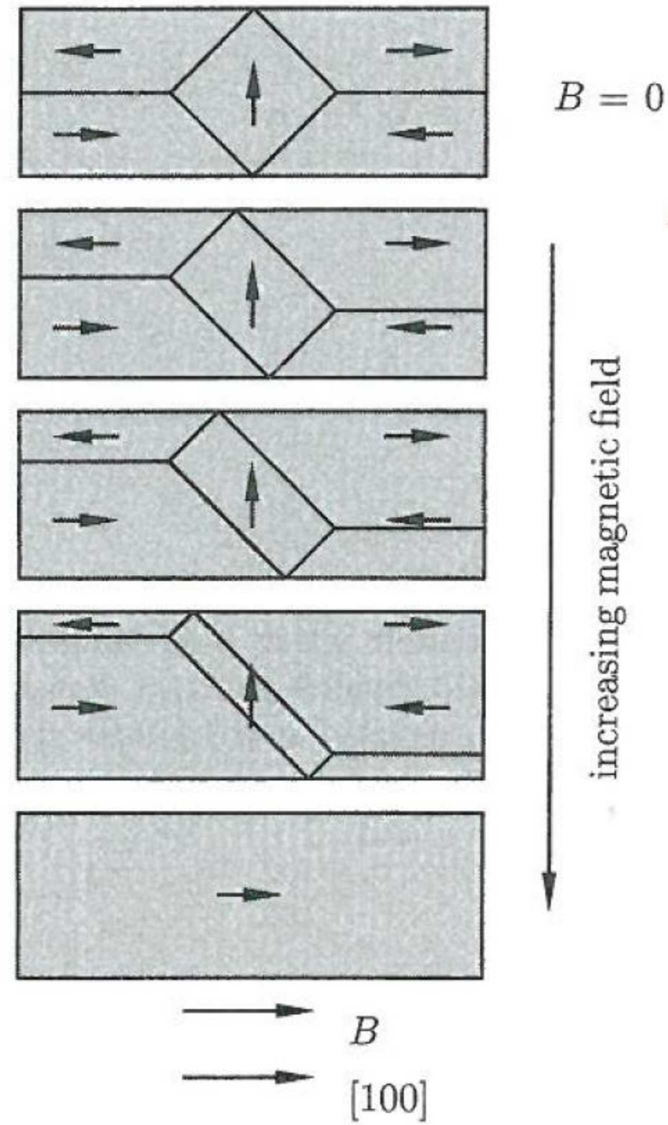

Fig. 6.25 Effect of an applied field on the domain pattern on the surface of a single crystal iron whisker showing domain wall displacement, as the applied B field increases from 0 up to a maximum value.

Vibrating sample magnetometer (VSM)

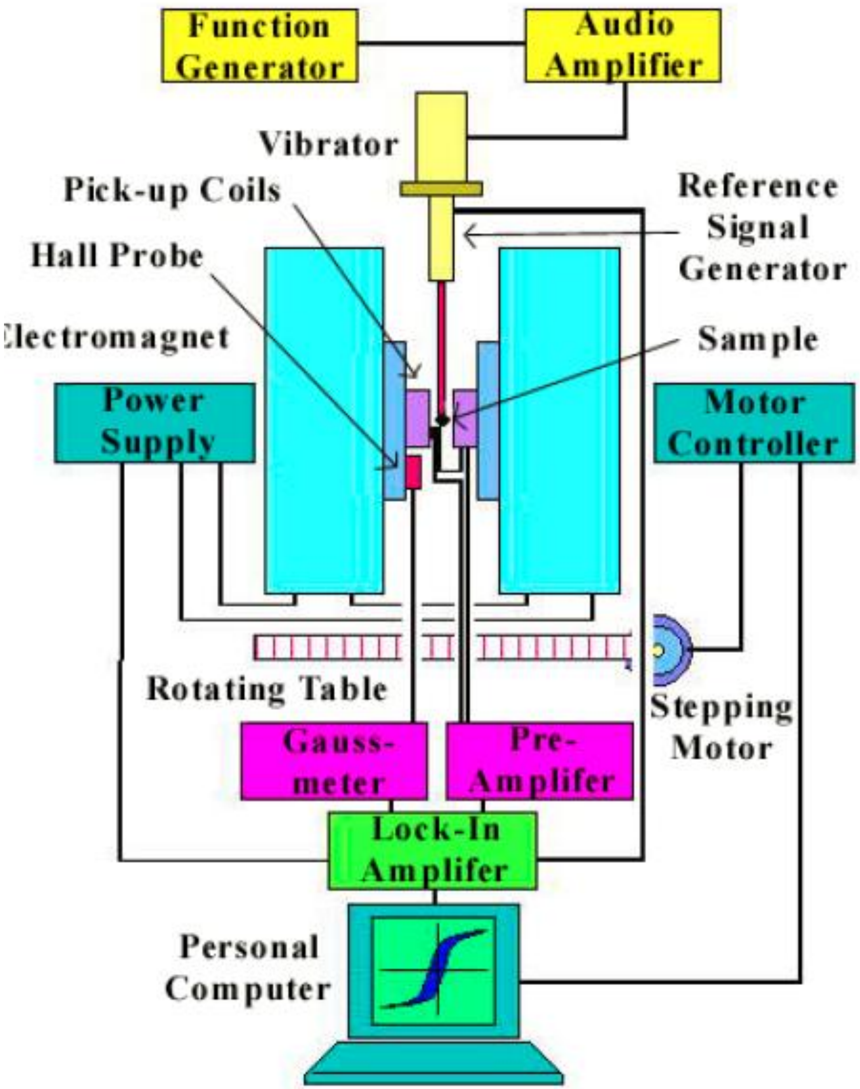

System diagram of
Vibrating Sample Magnetometer

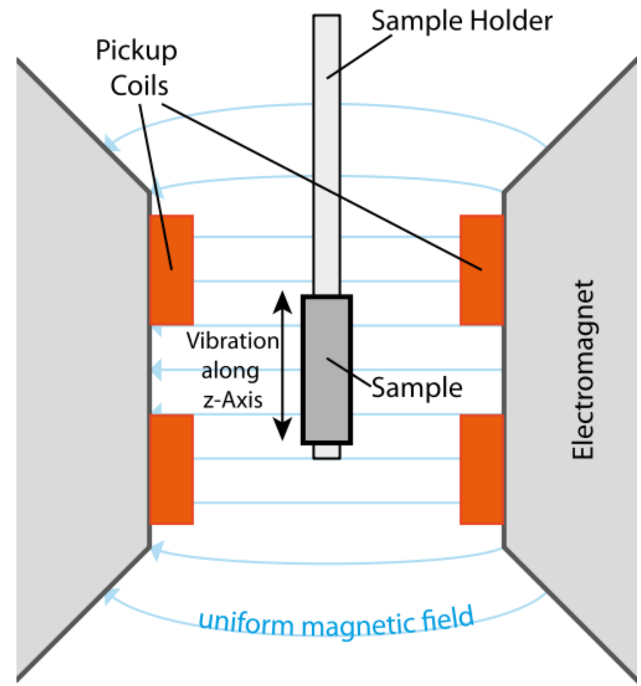

$$U = -N\dot{\Phi} \propto MV\dot{x}$$

SQUID

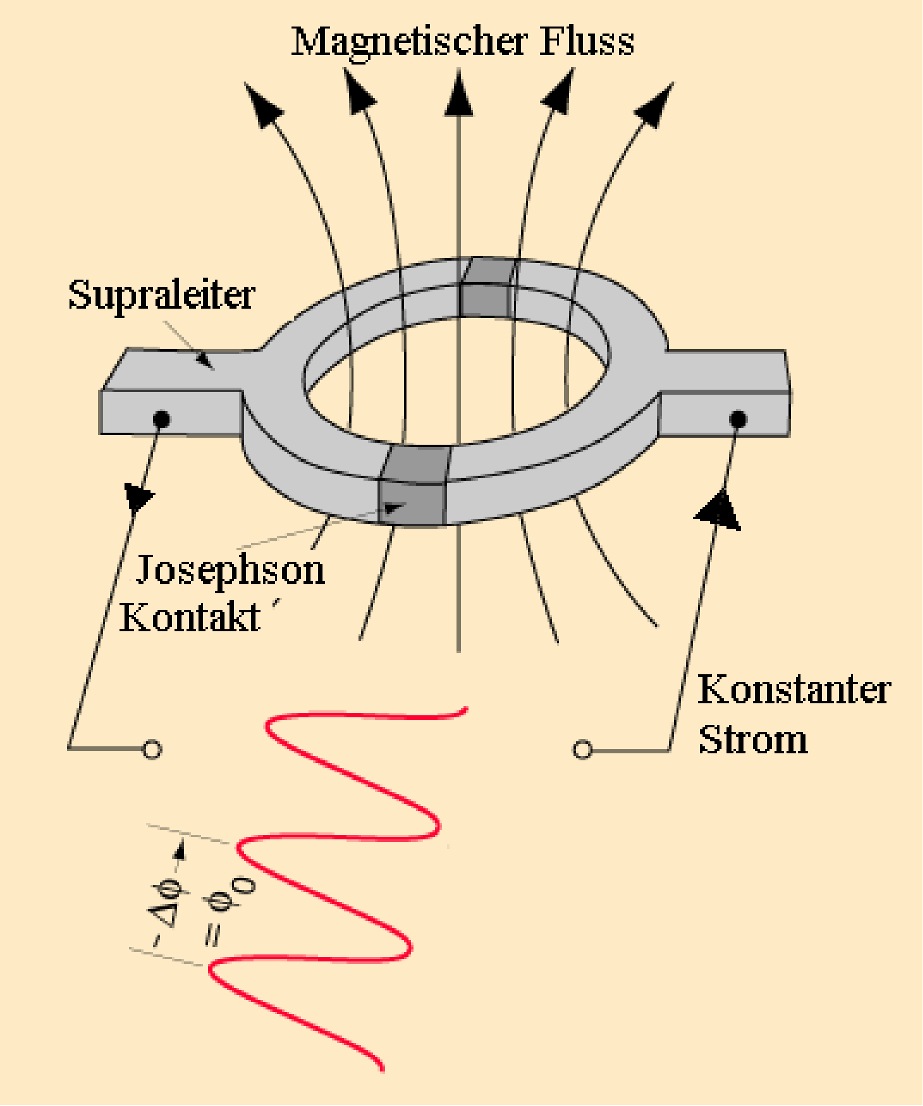
Magnetischer Fluss
Supraleiter
Josephson
Kontakt
Konstanter
Strom
$\Delta\Phi = \Phi_0$

EuO facts

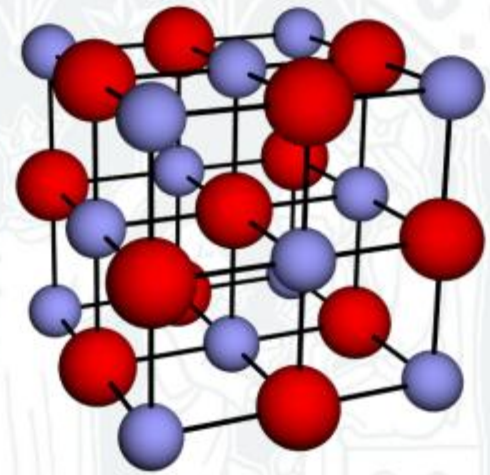

- Ionic rocksalt structure
- Ferromagnetic semiconductor, T_C = 69 K
- T_C increased up to 125 K by doping with Gd
- Colossal magnetoresistance (CMR)
- Photoconductivity
- Large magneto-optical Kerr effect (MOKE): Kerr rotation 7.1°
- Almost 100 % spin polarisation of the charge carriers [1]
- **Metal insulator transition (MIT) in EuO_{1-x} with $\Delta R/R$ up to 1000**

[1] H. Ott, S. J. Heise, R. Sutarto, Z. Hu, C. F. Chang, H. H. Hsieh, H.-J. Lin, C. T. Chen, and L. H. Tjeng *Phys. Rev. B* **73**, 094407 (2006)

SQUID-example: EuO

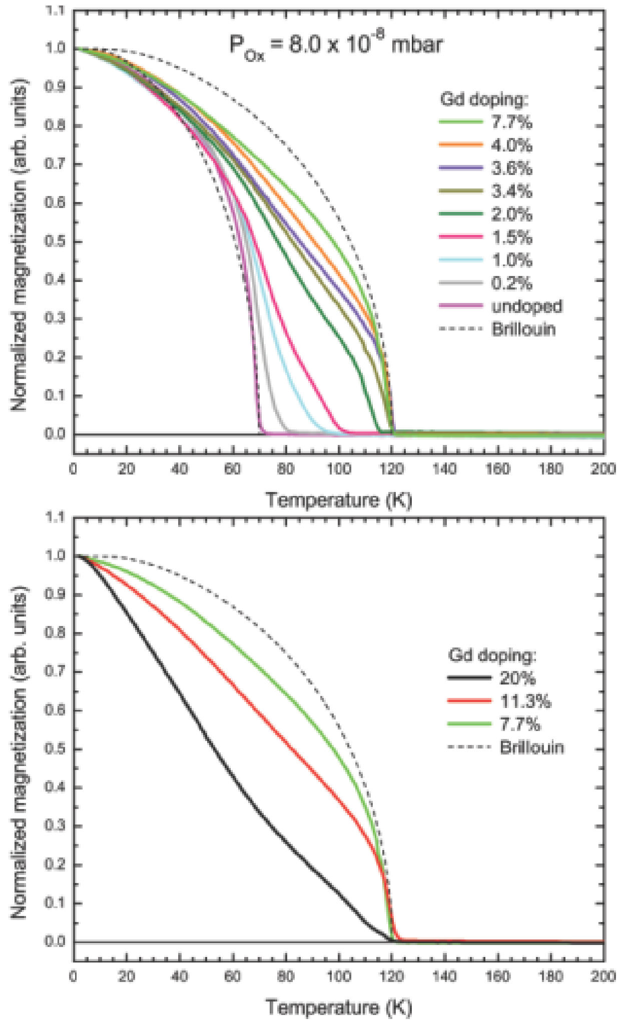

Figure 5.2: Temperature dependence of the normalized magnetization of epitaxial Gd-doped EuO films on YSZ (001) for various Gd concentrations from undoped to 7.7 % (*top panel*) and from 7.7 % to 20 % (*bottom panel*). The SQUID measurements were performed at applied magnetic field of 10 G. Taken from [17].

Magneto-optical effects

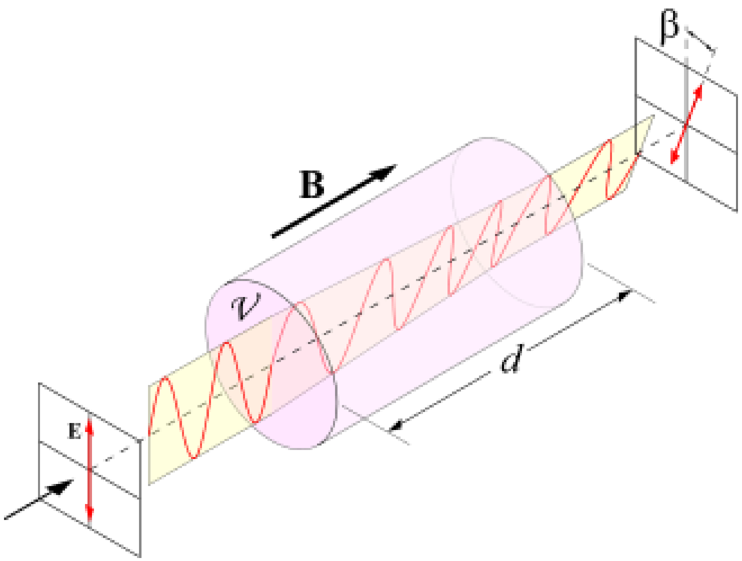

Faraday-effect

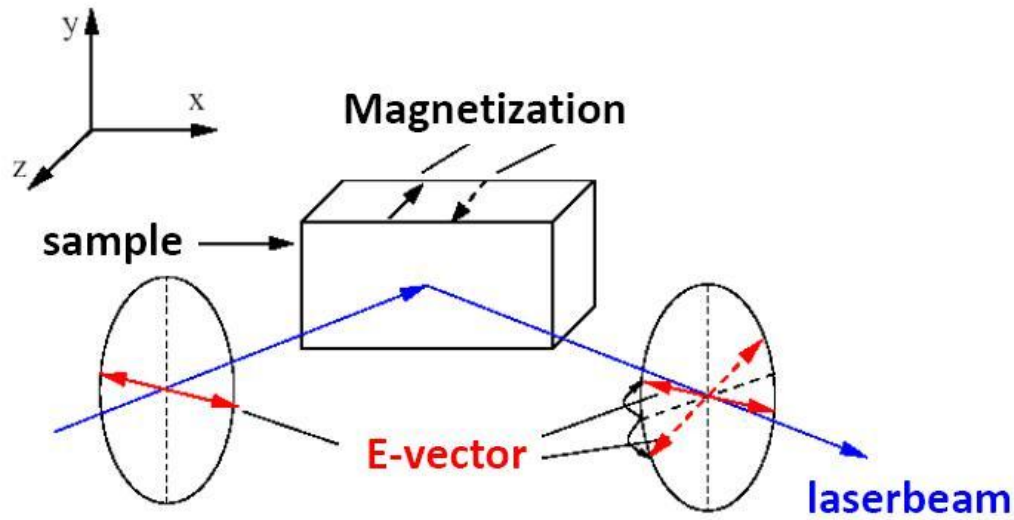

Kerr-effect

MOKE experimental setup

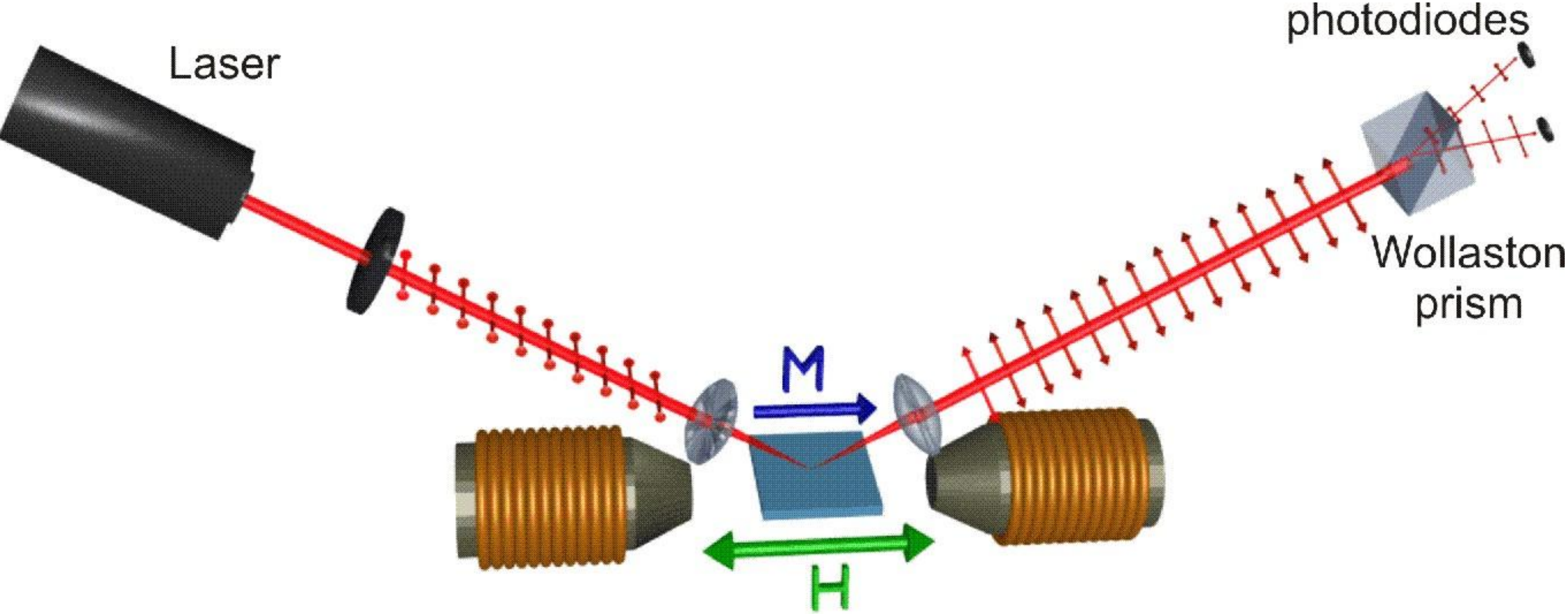

MOKE: sketch of measurement

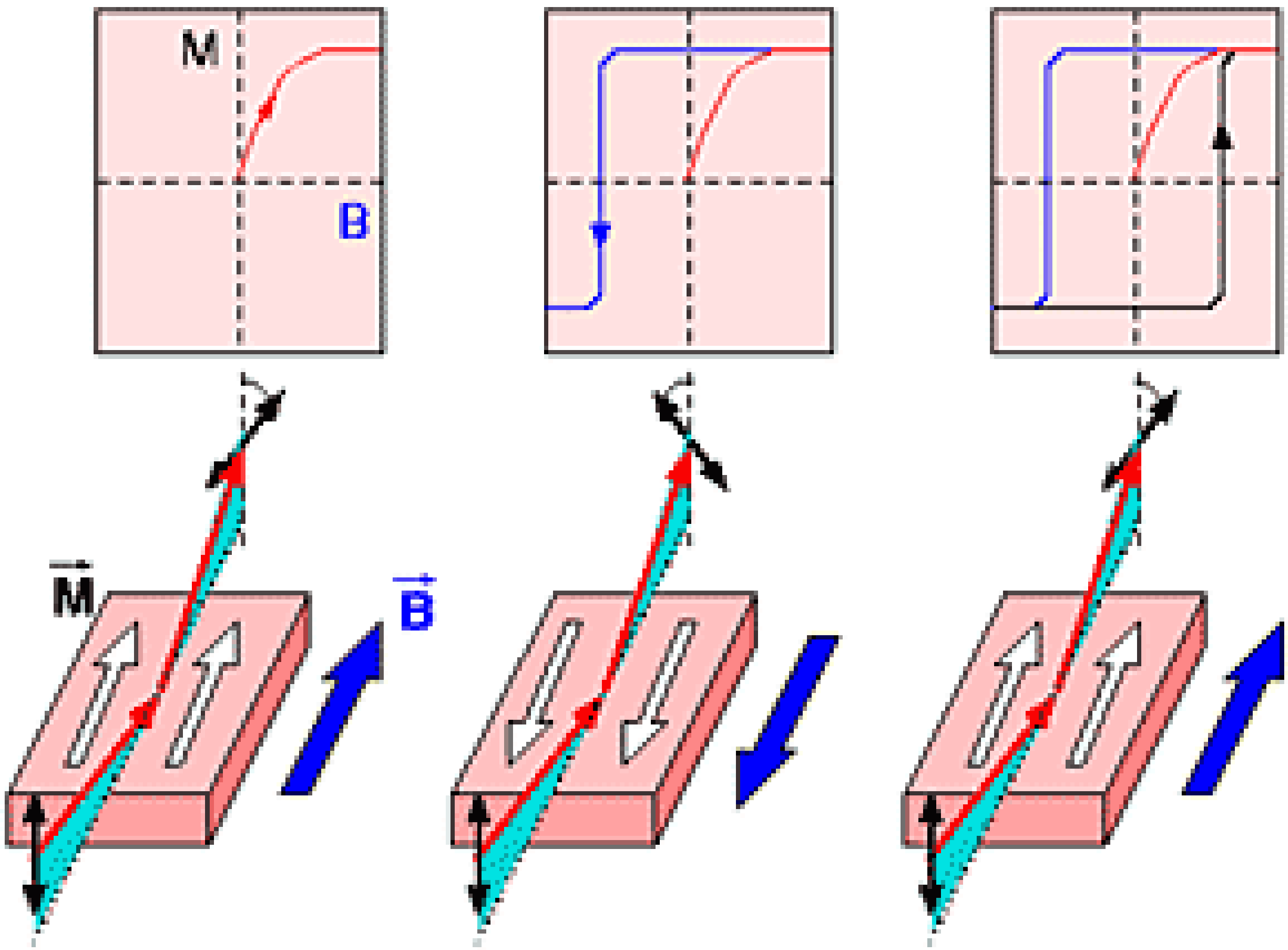

MOKE microscope

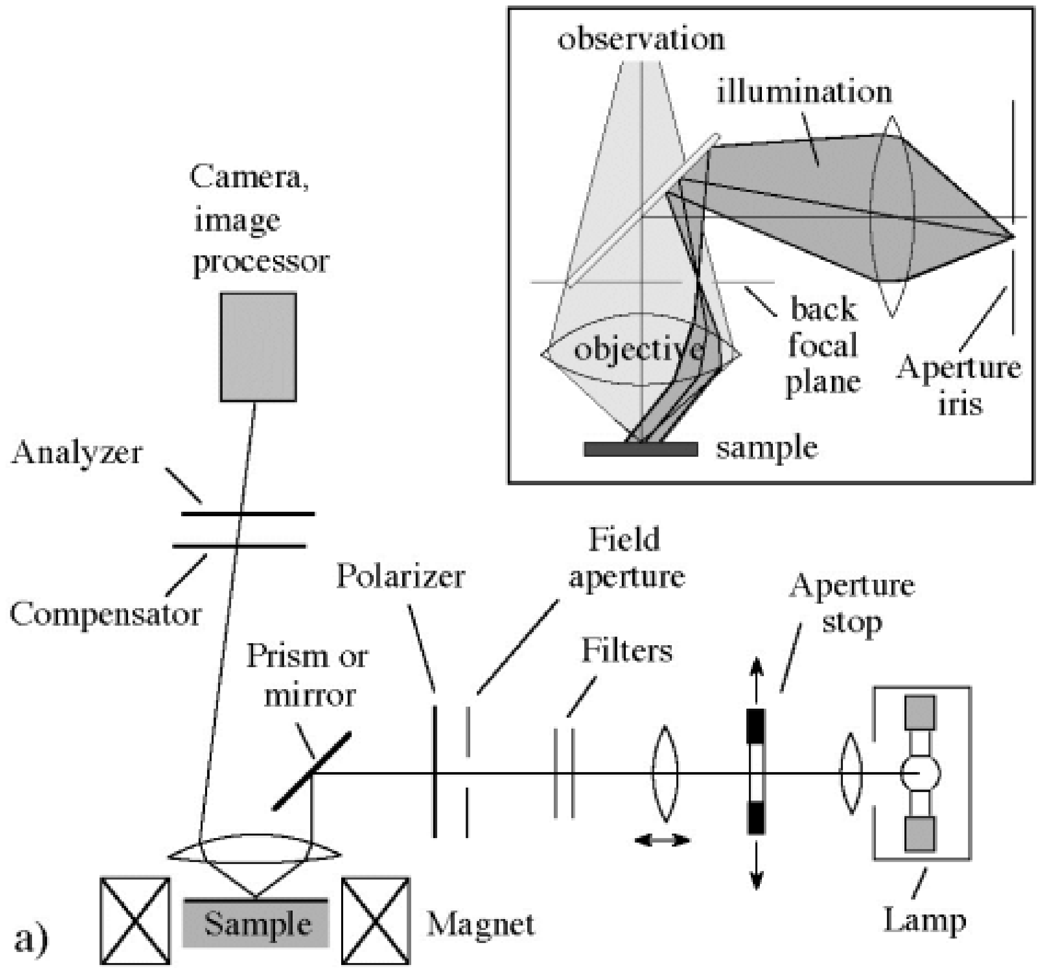

Fig. 6 Schematic representation of the main components of a magneto-optical Kerr microscope. The inset shows the beam path of an optical reflected light microscope. The aperture iris is displaced from the optical axis to generate oblique incidence of light.

$Nd_2Fe_{14}B$

MOKE microscope